Laser with thresholdless intensity fluctuations

N. J. van Druten, Y. Lien, C. Serrat, S. S. R. Oemrawsingh, M. P. van Exter, and J. P. Woerdman
Huygens Laboratory, Universiteit Leiden, P.O. Box 9504, Leiden, The Netherlands
(Received 27 September 1999; revised manuscript received 29 March 2000; published 17 October 2000)

We have studied the quantum-noise properties of a small slow-inversion laser experimentally and theoretically. As a function of pump rate, the average output intensity shows a sharp threshold, but the intensity fluctuations do not. Under quite generic conditions the intensity fluctuations of a sufficiently small slow-inversion laser show highly super-Poissonian statistics (even two times above threshold), due to the very weak damping of the spontaneous-emission-driven relaxation oscillation.

PACS number(s): 42.50.Lc, 05.70.Fh, 42.55.Sa

I. INTRODUCTION

One of the key features of any laser is its threshold. Most standard treatments of laser threshold (see, e.g., Refs. [1–3]) use a so-called class-A [4] description, i.e., the gain medium is assumed to be sufficiently fast that it may be adiabatically eliminated. It can then be shown that laser threshold characteristics are determined by a single parameter β, the fraction of the spontaneous emission going into the lasing mode [5]. For conventional ($\beta \ll 1$) lasers, including the great majority of current microlasers, threshold manifests itself in two ways: when the pump power is increased, (i) the average output into the lasing mode increases suddenly and (ii) the relative intensity fluctuations drop dramatically, from the thermal level below threshold to near the shot-noise level above threshold. The relative width of the threshold region defined according to (i) or (ii) is on the order of $\beta^{1/2}$. When the size of a laser is reduced, fewer modes of the electromagnetic field will be available for spontaneous emission, and β will increase. There is considerable current interest in such microlasers, both from a fundamental and from a practical point of view [6]. When approaching the $\beta=1$ limit, the threshold concept becomes illdefined with respect to both (i) and (ii). Hence lasers with large β are often referred to as ''thresholdless'' lasers [5].

We report here experiments which demonstrate that, contrary to the above standard treatment, under quite generic conditions the laser fluctuation threshold can disappear even for $\beta \ll 1$, although the *average* output intensity still exhibits a well-defined threshold. In our single-mode laser, the fluctuations remain at the thermal level even two times above threshold. We show theoretically that this behavior occurs when the inversion dynamics are too slow to efficiently damp the effects of the quantum-noise source, and demonstrate how this can be quantitatively understood via a class-B [4] description of the quantum-noise-driven laser dynamics. We thus find that this surprising behavior is an inherent property of any slow-inversion laser that is sufficiently small (i.e., has a sufficiently large β), see condition (13) below.

The outline of this paper is as follows. We start in Sec. II by describing the experimental setup. This will also serve to set the stage, introducing typical magnitudes for the laser parameters that we will be interested in. Next, we describe the theory in Sec. III, in particular focusing on the parameter values introduced in Sec. II. We start with the case of an ideal four-level laser in Sec. III A. This allows us to discuss many of the relevant aspects within the simplest possible framework. To quantitatively describe our experimental data a more detailed model is needed; specifically the lower-level dynamics needs to be taken into account. The extended theory is described in Sec. III B. In Sec. IV we then present the experimental data and compare them to the results of the theory. We close in Sec. V with a discussion of our results and some conclusions.

II. EXPERIMENTAL SETUP

The laser configuration used in our experiments is indicated in Fig. 1. It consists of a coated, 0.2-mm-thin Nd:YVO_4 laser crystal (a ''microchip'' [7]), combined with a concave output coupler with a 25-mm radius of curvature. The *a*-cut Nd:YVO_4 crystal has a specified doping of 1% atomic Nd, and a refractive index $n_e=2.17$ at 1064 nm [8]. The output coupler, with a measured reflectivity $R_m=80\%$ at 1064 nm, is placed as close as possible (≈ 0.1 mm) to the laser crystal. The microchip laser is optically pumped using the intensity-stabilized output of a titanium-sapphire laser operating at 808 nm. The root-mean-square intensity fluctuations of the pump light are less than 0.1%.

Nd:YVO_4 has a homogeneously broadened laser transition at 1064 nm. The fluorescence at 1064 nm of our laser crystal was measured to have a near-Lorentzian spectrum with a full width at half-maximum (FWHM) of $\gamma_\perp/\pi = 0.22(2)$ THz, while the decay rate of the upper laser level was determined as $\gamma_\parallel = 1.3(1)\times 10^4$ s^{-1}. The lower-level decay rate γ_b is very much larger, 1.6×10^9 s^{-1} [9], hence

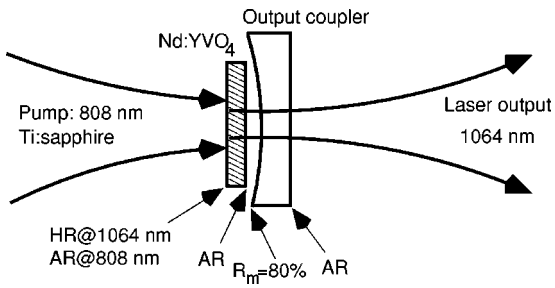

FIG. 1. Laser configuration used in the experiments (not to scale). The laser cavity is formed by the concave surface of the output coupler and the pump-side surface of the Nd:YVO_4 laser crystal. The dielectric coatings are indicated, HR for highly reflective, AR for antireflection coating.

the 1064-nm transition in Nd:YVO_4 is generally considered to be an ideal four-level laser transition. The length of the microchip laser cavity could be piezoelectrically tuned. By detuning the cavity away from gain maximum, the microchip laser could be made to lase in two longitudinal modes. The typical longitudinal mode spacing found in this way, using a tunable planar Fabry-Perot interferometer, was $c/2l_{\rm opt}=0.27(3)$ THz, so that we deduce an optical cavity length $l_{\rm opt}=0.56(5)$ mm, consistent with the lengths given above. From the cavity parameters we estimate the cavity loss rate to be $\Gamma_c=-(c/2l_{\rm opt})\ln R_m=6\times10^{10}$ s^{-1}, and, using the results in Ref. [10], $\beta=2\times10^{-5}$. For the experimental data presented here, the microchip cavity was tuned so that the cavity resonance coincided with gain maximum, and we verified that the microchip laser operated in a single transverse and longitudinal mode using the Fabry-Perot interferometer. The laser output at 1064 nm was sent through an optical isolator and detected on a calibrated InGaAs photodetector (effective bandwidth 20 MHz).

III. THEORY

In this section we give the theory needed to describe the intensity noise of a slow-inversion laser. We will concentrate on the photon number fluctuations normalized in the two ways that are commonly used [1–3,5], namely, the normalized variance, known as the Fano factor $F=\langle\delta n^2\rangle/\langle n\rangle$, and the reduced factorial moment $Q_2=(F-1)/\langle n\rangle\approx\langle\delta n^2\rangle/\langle n\rangle^2$. The Fano factor normalizes the intensity fluctuations to the shot-noise level, $F=1$ for a Poissonian distribution. In usual lasers, F is of order unity both above and below threshold, and shows a sharp peak at threshold, $M=1$, with a width of $\approx\beta^{1/2}$ in M, and a height of $\approx(4\beta)^{-1/2}$ [see Fig. 4(b)], where M is the normalized pump parameter. The reduced factorial moment Q_2 normalizes the intensity fluctuations to those in a single mode of a thermal field, $Q_2=1$ for the Planck distribution in a single optical mode, while $Q_2=0$ for a Poissonian distribution. In usual lasers, the reduced factorial moment Q_2 drops steeply from one to zero in the same threshold range ($Q_2=1/2$ is reached at $M=1$) with a width $\approx\beta^{1/2}$ [see Fig. 4(a)]. Note that $Q_2=g_2(0)-1$, with g_2 the normalized second-order coherence function [2].

We start in Sec. III A with the simplest case, and use it to derive simple expressions for the intensity noise properties for a laser around threshold. The standard results for the intensity noise around laser threshold are recovered only for a limited range of laser parameters, and two new regimes are identified. Although the key elements of this analysis can be traced back to the early work of McCumber [11] and Lax [12], the consequences for the noise threshold seem to have been overlooked so far. Recently, a similar analysis was independently developed by Hofmann and Hess [13,14] who focused on the relevance for semiconductor lasers. Next, in Sec. III B, the theory is extended to include the lower-level dynamics, which will turn out to be important for a quantitative understanding of the experimental data.

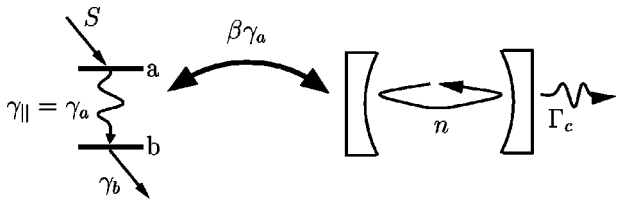

FIG. 2. Schematic overview of the relevant coupling and decay rates of the laser considered here, see Eqs. (1) and (20). The upper laser level, a, is pumped at a rate S, and decays by spontaneous emission at a rate $\gamma_a=\gamma_\parallel$ to the lower laser level b which decays at γ_b. A fraction β of the spontaneous emission couples to the mode in the optical cavity that is lasing for sufficiently strong pump S. The number of photons in that mode is denoted by n, and the ''cold'' cavity decay rate is denoted by Γ_c. For the ideal four-level case, Eqs. (1), the lower-level decay rate γ_b is assumed to be sufficiently large that the lower level population can be neglected.

A. Ideal four-level laser

We limit ourselves here to a single-mode laser with a homogeneously broadened gain medium operated at gain maximum in the good-cavity regime ($\gamma_\perp\gg\Gamma_c$), and not too far above threshold where spontaneous emission is the main source of quantum noise. The level structure and relevant rates are schematically indicated in Fig. 2. In this section, we consider the case of an ''ideal four-level'' laser, i.e., the decay rate γ_b of the lower laser level is assumed to be sufficiently large that the lower-level population can be completely neglected.

For such a laser, the following rate equations for the intracavity photon number n and the inversion N (number of upper-level atoms) can be derived from the laser Maxwell-Bloch equations [15]

$$\dot{n}=-\Gamma_c n+\beta\gamma_\parallel Nn+R_{\rm sp}+f_n, \tag{1a}$$

$$\dot{N}=S-\gamma_\parallel N-\beta\gamma_\parallel Nn, \tag{1b}$$

where S is the pump rate, $R_{\rm sp}=N\beta\gamma_\parallel$ is the spontaneous emission rate into the lasing mode, and Γ_c, β, and $\gamma_\parallel$ have been defined above. The Langevin noise source f_n represents the quantum noise associated with spontaneous emission, and satisfies $\langle f_n(t)f_n(t')\rangle=2R_{\rm sp}n\delta(t-t')$. The inversion noise source f_N has been neglected in Eq. (1b); this is discussed in some more detail in the Appendix.

The steady state (n_0,N_0) is readily calculated by neglecting f_n and setting the time-derivatives in Eqs. (1) equal to zero. This yields

$$N_0=\frac{\Gamma_c}{\beta\gamma_\parallel}\frac{n_0}{n_0+1}, \tag{2a}$$

$$\frac{M}{1+\beta n_0}=\frac{n_0}{n_0+1}, \tag{2b}$$

with $M=S\beta/\Gamma_c$ the normalized pump rate. From Eq. (2b) one directly finds the well-known result [1–3,5]

$$n_0=\frac{1}{\beta}\left[\frac{M-1}{2}+\sqrt{\left(\frac{M-1}{2}\right)^2+\beta M}\right]. \tag{2c}$$

As long as $\beta \ll 1$, n_0 shows a sharp increase at $M=1$, defining the common threshold in the average output intensity. Equation (2c) also shows that the laser threshold in n_0 has a sharpness of order $\beta^{1/2}$ in the pump parameter M.

Turning now to the fluctuations, we write $n=n_0+\delta n$ and $N=N_0+\delta N$, and linearize Eqs. (1) around steady state. This yields

$$\dot{\delta n} = -\gamma_n \delta n + \beta \gamma_\parallel (n_0+1)\,\delta N + f_n, \tag{3a}$$

$$\dot{\delta N} = -\gamma_\parallel N_0 \beta\, \delta n - \gamma_N \delta N. \tag{3b}$$

The fluctuations in photon number and inversion are both intrinsically damped, so that the steady state found above is indeed a stable solution, as is well-known for a class-B laser [4]. The damping rates are the ''photonic damping'' $\gamma_n = R_{\rm sp}/n_0 = \Gamma_c/(n_0+1)$ and the ''atomic damping'' $\gamma_N = \gamma_\parallel(1+\beta n_0)$, respectively. The atomic damping rate represents the net stabilizing effect of the inversion on the laser dynamics. The photonic damping is the net damping rate of the ''loaded'' cavity. It is directly related to the presence in Eq. (1a) of the nonzero average spontaneous-emission rate $R_{\rm sp}$, and hence to the strength of the quantum noise f_n. Above threshold it is usually negligible, i.e., the loss rate of the empty cavity Γ_c is nearly compensated for by the gain term in Eq. (1a). However, in our case the photonic damping is nevertheless important, since it may dominate over the (even smaller) atomic damping. The strength of γ_n compared to γ_N will turn out to be of key importance for the threshold behavior of the intensity fluctuations.

Fourier transforming Eqs. (3), and inverting the resulting matrix (see also the Appendix), leads to

$$\langle \delta n^2(\omega)\rangle = \frac{2(\omega^2+\gamma_N^2)R_{\rm sp}n_0}{(\omega_{\rm ro}^2+\gamma_n\gamma_N-\omega^2)^2+4\omega^2\gamma_{\rm ro}^2} \tag{4}$$

for the double-sided spectral density $\langle \delta n^2(\omega)\rangle$ of the intensity fluctuations. Here, we have introduced the relaxation oscillation frequency $\omega_{\rm ro}$ and the relaxation-oscillation damping rate $\gamma_{\rm ro}$. The relaxation oscillation frequency $\omega_{\rm ro}$ is given by the product of the coupling terms in Eqs. (3), i.e.,

$$\omega_{\rm ro}^2 = \beta^2\gamma_\parallel^2 N_0(n_0+1) = \gamma_\parallel \Gamma_c \beta n_0, \tag{5}$$

where Eq. (2a) has been used for the second equality. The damping rate $\gamma_{\rm ro}$ of the relaxation oscillations is the average of the atomic damping γ_N and the photonic damping γ_n, $\gamma_{\rm ro}=(\gamma_N+\gamma_n)/2$. In this linearized model, in the regime $\omega_{\rm ro} \gg \gamma_{\rm ro}$ (as is typically the case for a class-B laser above threshold) the noise power spectrum of the photon number fluctuations peaks at $\omega_{\rm ro}$, with a width (FWHM) of $\Delta\omega_{\rm ro}=2\gamma_{\rm ro}$. Integrating Eq. (4) over frequency (see the formulas in the Appendix of Ref. [16]), leads to

$$\frac{\langle \delta n^2\rangle}{n_0^2} = \left(\frac{\gamma_n}{\gamma_n+\gamma_N}\right)\left(1+\frac{\gamma_N^2}{\omega_{\rm ro}^2+\gamma_n\gamma_N}\right), \tag{6}$$

which may be rewritten as

$$\frac{\langle \delta n^2\rangle}{n_0^2} = 1-\left(\frac{\omega_{\rm ro}^2}{\omega_{\rm ro}^2+\gamma_n\gamma_N}\right)\left(\frac{\gamma_N}{\gamma_N+\gamma_n}\right). \tag{7}$$

This is the central result of this section.

Our interest here is in a laser with $\beta \ll 1$ operated near threshold or above threshold ($M \gtrsim 1$) so that $n_0 \gtrsim \beta^{-1/2} \gg 1$, see Eq. (2c). Thus, we can neglect the subtleties associated with the difference between n_0+1 and n_0, and may write $Q_2=(F-1)/n_0 \approx \langle \delta n^2\rangle/n_0^2$, i.e., Eq. (7) directly gives both Q_2 and F. The appeal of Eq. (7) is that it shows directly that the noise level only drops much below the thermal level of $Q_2=1$ when *two* conditions are met, namely, $\omega_{\rm ro}^2 > \gamma_n\gamma_N$ and $\gamma_N > \gamma_n$. Thus, the fluctuation threshold can be discussed in terms of two dimensionless ratios, namely,

$$\frac{\omega_{\rm ro}^2}{\gamma_n\gamma_N} \approx \frac{\beta n_0^2}{1+\beta n_0} \tag{8}$$

and

$$\frac{\gamma_N}{\gamma_n} \approx \frac{\gamma_\parallel(1+\beta n_0)n_0}{\Gamma_c} = \frac{(1+\beta n_0)n_0}{\Lambda}, \tag{9}$$

where we have again neglected the difference between n_0+1 and n_0. Because of the importance of the ratio of atomic and photonic damping γ_N/γ_n we have introduced the shorthand notation

$$\Lambda = \Gamma_c/\gamma_\parallel \tag{10}$$

here. Λ is a measure of the ''slowness'' of the inversion.

The first of the above two conditions for Q_2 to drop below the thermal level, $\omega_{\rm ro}^2 > \gamma_n\gamma_N$, leads to $n_0 > \beta^{-1/2}$ [see Eq. (8), we assume $\beta \ll 1$] and thus coincides with the threshold defined via the steady-state photon number, since $n_0=\beta^{-1/2}$ at $M=1$. This is the conventional intensity-noise threshold derived in textbooks [1–3], using a class-A treatment. There, the inversion dynamics is adiabatically eliminated, and thus it is assumed that the atomic damping is much larger than the photonic damping $\gamma_N \gg \gamma_n$ around $M=1$. In other words, the inherent assumption in the standard treatment is that the photonic damping $\gamma_n=\Gamma_c/(n_0+1)$ is sufficiently *suppressed* (via the increased photon number n_0) around threshold that it is negligible compared to the atomic damping $\gamma_N \approx \gamma_\parallel$. However, Eq. (9) shows that this assumption need not be valid. In fact, in our experiment $\Lambda \approx 4\times 10^6$ and $\beta \approx 10^{-5}$, so that $\gamma_N \ll \gamma_n$ around threshold, and the photonic damping *dominates* over the atomic damping even considerably above threshold.

More generally, three different regimes for the threshold behavior of the intensity fluctuations can now be distinguished, using the ratios in Eqs. (8) and (9). These regimes have also been identified by Hofmann and Hess [14], and we adopt their nomenclature here.

(1) The macroscopic regime:

$$\beta < \Lambda^{-2}, \tag{11}$$

where the laser shows the conventional noise threshold.

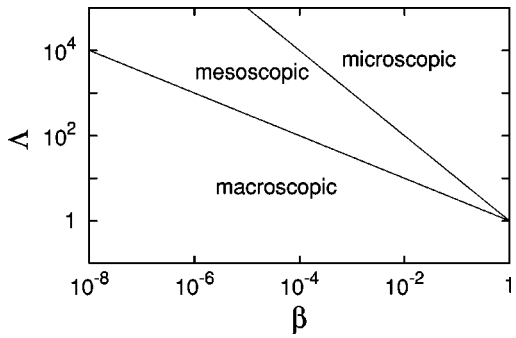

FIG. 3. Overview of the different regimes for the fluctuation threshold, in terms of β and $\Lambda=\Gamma_c/\gamma_\parallel$. The solid lines correspond to inequalities (11) and (13), respectively.

(2) The mesoscopic regime:

$$\Lambda^{-2}<\beta<\Lambda^{-1}, \tag{12}$$

where the noise threshold is significantly modified from the conventional case, but still remaining relatively sharp.

(3) The microscopic regime:

$$\beta>\Lambda^{-1}, \tag{13}$$

where the intensity fluctuations effectively become thresholdless.

The three regimes defined above are indicated in the ''phase diagram'' of Fig. 3, and examples of the typical behavior of both Q_2 and F in these regimes are shown in Fig. 4. We end this section by discussing these three regimes in some more detail.

In the macroscopic regime, the atomic damping dominates over the photonic damping around the steady-state threshold. This can directly seen as follows: for $M=1$ one has $n_0=\beta^{-1/2}$, and in the macroscopic regime this implies, using Eq. (11), $n_0>\Lambda$, leading to $\gamma_N>\gamma_n$, using Eq. (9). Thus, as the photon number is increased the condition $\gamma_N>\gamma_n$ is reached before $\omega_{\rm ro}^2>\gamma_n\gamma_N$. This is the basic assumption in the conventional, class-A treatment of laser threshold, and the results of this conventional treatment are recovered. In fact, since for a class-A laser $\Gamma_c<\gamma_\parallel$ $(\Lambda<1)$ and by definition $\beta\leqslant 1$, all class-A lasers satisfy Eq. (11) and operate in the ''macroscopic'' regime. In Eq. (7) we may now use $\gamma_N/(\gamma_n+\gamma_N)\approx 1$, resulting in

$$Q_2\approx\frac{\gamma_n\gamma_N}{\omega_{\rm ro}^2+\gamma_n\gamma_N}. \tag{14}$$

The noise behavior is completely determined by the ratio in Eq. (8), and hence leaves β as the only parameter. The noise level drops from the thermal level $(Q_2=1)$ to $Q_2\approx 0$ in a narrow region of width $\approx\beta^{-1/2}$ around $M=1; Q_2=1/2$ at $M\approx 1$. The Fano factor $F=n_0Q_2+1$ exhibits a narrow peak at the same value where $Q_2=1/2$, around $M=1$, with a width $\approx\beta^{-1/2}$, and a peak value

$$F_{\rm max}\approx(4\beta)^{-1/2} \quad \text{at} \quad M\approx 1. \tag{15}$$

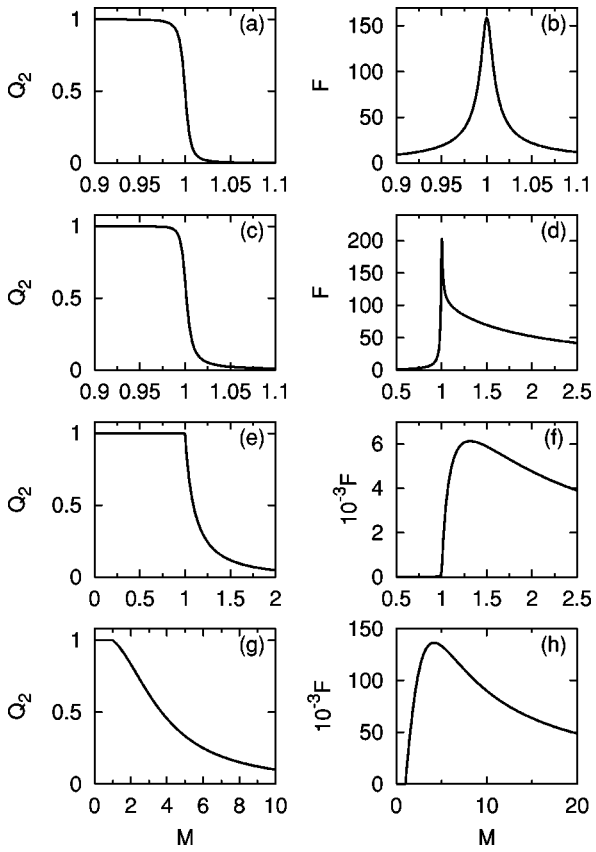

FIG. 4. Laser noise threshold behavior in different regimes. The graphs show typical curves for the reduced factorial moment Q_2 and the Fano factor F as a function of pump parameter M, in the different regimes discussed in the text, see also Fig. 3. Note the changes in horizontal and vertical scales. In these graphs $\beta=10^{-5}$, while $\Lambda=\Gamma_c/\gamma_\parallel$ is varied: (a), (b) $\Lambda=1$, (c), (d) $\Lambda=100$, (e), (f) $\Lambda=10^4$, (g), (h) $\Lambda=10^6$. (a), (b): the conventional laser noise threshold. (c) and (d): approach to the ''mesoscopic'' regime, Q_2 is hardly changed, while the Fano factor is already significantly modified. (e) and (f): the ''mesoscopic'' regime; the threshold in Q_2 is shifted somewhat, while the Fano factor exhibits a very broad peak. (g) and (h): ''microscopic'' regime, where the intensity fluctuations have effectively become thresholdless: both Q_2 and F have a very broad shape.

Typical shapes of both Q_2 and F in this regime are indicated in Fig. 4(a)–(d). These were calculated using Eq. (7).

In the mesoscopic regime, there is a narrow region above $M=1$ where the atomic damping is still smaller than the photonic damping. The point $\gamma_N=\gamma_n$ is reached for $n_0\approx\Lambda$, i.e., for n_0 in the range $\beta^{-1/2}<n_0<\beta^{-1}$ [as can be directly verified using Eqs. (9) and (12)]. According to Eq. (7), Q_2 will only deviate significantly from the thermal value 1 when $\gamma_N\gtrsim\gamma_n$, i.e., when $n_0\gtrsim\Lambda$. Since this implies $n_0>\beta^{-1/2}$ and hence $\omega_{\rm ro}^2>\gamma_n\gamma_N$ [see Eq. (8)], we may use $\omega_{\rm ro}^2/(\omega_{\rm ro}^2+\gamma_n\gamma_N)\approx 1$ in the expression for Q_2 in Eq. (7), resulting in

$$Q_2\approx\frac{\gamma_n}{\gamma_N+\gamma_n}. \tag{16}$$

Thus, in this regime the noise behavior is determined by the

ratio in Eq. (9). As a consequence, β is now no longer the only parameter that describes the noise threshold; the second parameter is Λ.

Simple expressions for both Q_2 and F in terms of the pump parameter M, are now obtained by using the approximation $n_0 \approx (M-1)/\beta$. This is justified since the relevant structure in both Q_2 and F occurs for $n_0 > \beta^{-1/2}$, i.e., for $M>1$. With this approximation we find that $Q_2=1/2$ at $M=1+\Lambda\beta$, and Q_2 drops from the thermal level to zero in a narrow range $\Delta M=\Lambda\beta$ centered around this value. The threshold behavior of Q_2 is thus changed as compared to the ''macroscopic'' case, it has broadened and shifted. In comparison, the Fano factor F changes much more drastically. It becomes highly asymmetric, rising steeply for pump parameters $M \gtrsim 1$, reaching a peak value

$$F_{\max} \approx \Lambda \quad \text{at} \quad M \approx 1+(\Lambda\beta)^{1/2}, \tag{17}$$

and dropping slowly as $F \approx \Lambda/M$ for larger M values. Note that $F_{\max}$ no longer coincides with $Q_2=1/2$ in this regime. Typical shapes of both Q_2 and F in this regime, calculated using the full expression (7), are shown in Figs. 4(e), 4(f).

In the microscopic regime the atomic damping remains smaller than the photonic damping up to M values much larger than 1. Thus, the laser light fluctuates at the thermal level $Q_2 \approx 1$ even for M considerably larger than 1. The equality $\gamma_N=\gamma_n$ is reached only for $n_0 > 1/\beta$ [see Eqs. (9) and (13)]. As in the mesoscopic regime, since we have $\omega_{\mathrm{ro}}^2 \gg \gamma_n\gamma_N$ in the range of interest, Eq. (16) is an excellent approximation to Eq. (7), and the ratio in Eq. (9) determines the threshold behavior. Since $\gamma_N \gtrsim \gamma_n$ is reached only for $\beta n_0 > 1$, Eq. (9) may be approximated as

$$\gamma_N/\gamma_n \approx \beta n_0^2/\Lambda \tag{18}$$

in the range of interest. With this approximation one finds that $Q_2=1/2$ is reached at $n_0 \approx (\Lambda/\beta)^{1/2}$, i.e., at $M \approx 1+(\Lambda\beta)^{1/2} \gtrsim 2$. In contrast to the mesoscopic regime, but similar to the microscopic regime, the point $Q_2=1/2$ coincides with the pump power where the maximum Fano factor is reached,

$$F_{\max} \approx (\Lambda/4\beta)^{1/2} \quad \text{at} \quad M \approx 1+(\Lambda\beta)^{1/2}. \tag{19}$$

In the microscopic regime both Q_2 and F have a very broad shape, and there is no longer a well-defined threshold in the intensity fluctuations, see Figs. 4(g) and 4(h).

As a final remark we emphasize that the transitions between these regimes are not abrupt but smooth. For instance, Fig. 4(d) shows that the Fano factor already deviates from the conventional, ''macroscopic'' laser theory before the mesoscopic regime is reached.

B. Including the lower level

To properly describe our experiments on Nd:YVO_4 microchip lasers, we need to extend the laser rate equations, with a dynamic equation for the lower-level population:

$$\dot{n} = -\Gamma_c n + \beta\gamma_a(N_a-N_b)n + R_{\mathrm{sp}} + f_n, \tag{20a}$$

$$\dot{N}_a = S - \gamma_a N_a - \beta\gamma_a(N_a-N_b)n, \tag{20b}$$

$$\dot{N}_b = -\gamma_b N_b + \gamma_a N_a + \beta\gamma_a(N_a-N_b)n, \tag{20c}$$

where $R_{\mathrm{sp}}=N_a\beta\gamma_a$ and N_a and N_b are the number of upper- and lower-level atoms, respectively, with decay rates γ_a ($\equiv\gamma_\parallel$) and γ_b. The quantities β, n, and Γ_c have been defined above. The Langevin noise source f_n satisfies once again $\langle f_n(t) f_n(t')\rangle = 2R_{\mathrm{sp}} n\,\delta(t-t')$.

We will not attempt a full solution to Eqs. (20) here, but will limit ourselves to the regime ($\gamma_b \gg \gamma_a$) in which the experiments were performed. Equation (20c) yields for the steady-state lower-level population $N_{b,0}$

$$N_{b,0} = N_{a,0}\frac{\gamma_a(1+\beta n_0)}{\gamma_b+\gamma_a\beta n_0}. \tag{21}$$

Because of the rapid decay rate of the lower level, $\gamma_b \gg \gamma_a$, $N_{b,0}$ is quite small compared to $N_{a,0}$. Its effect is sufficiently small that the steady-state photon number n_0 and the relaxation oscillation frequency ω_{ro} are basically unaffected. However, the dependence of $N_{b,0}$ on n_0 leads, via the gain term $\beta\gamma_a(N_a-N_b)n$ in Eq. (20a) to a small ''nonlinear gain'' for the photon number, that will be important for the fluctuations. From semiconductor laser studies it is in fact well-known that such nonlinear gain can be important for the laser dynamics [17,18].

To calculate the intensity fluctuations, we first adiabatically eliminate the dynamics of the lower level, setting $\dot{N}_b=0$. This is allowed as long as $\gamma_b \gg \gamma_a, \omega_{\mathrm{ro}}$, a condition that is readily satisfied in our experiments. As an aside we note here that since we deal now once again with only two dynamical variables, the instabilities associated with higher-dimensional laser dynamics are still absent [4].

Linearizing the remaining Eqs. (20a) and (20b) around the steady-state solution yields coupled linear equations for the fluctuations δn and δN_a nearly identical to Eqs. (3), except for one significant modification: the photon damping term γ_n in Eq. (3a) is replaced by $\gamma_n+\gamma_{\mathrm{NL}}$, where γ_{NL} is an additional ''atomic'' damping term caused by lower-level dynamics, via the abovementioned nonlinear gain term

$$\gamma_{\mathrm{NL}} = \frac{\gamma_a\Gamma_c\beta n_0}{\gamma_b} = \frac{\omega_{\mathrm{ro}}^2}{\gamma_b}. \tag{22}$$

The rapid decay rate γ_b of the lower level (compared to γ_a of the upper level) causes the lower-level population to be small, but at the same time allows for very rapid dynamics of part of the atomic inversion. The net result is that in the atomic damping rate the lower-level dynamics may dominate over the upper-level dynamics, $\gamma_{\mathrm{NL}} \gg \gamma_N$ even though the lower-level population is negligible for the steady-state behavior.

The inclusion of γ_{NL} in Eqs. (3) leads to Eq. (4) with γ_n replaced by $\gamma_n+\gamma_{\mathrm{NL}}$ and with $\gamma_{\mathrm{ro}}=(\gamma_n+\gamma_{\mathrm{NL}}+\gamma_N)/2$. Thus we arrive at a result analogous to Eq. (6) namely,

$$\frac{\langle \delta n^2 \rangle}{n_0^2} = \left(\frac{\gamma_n}{\gamma_n + \gamma_N + \gamma_{\mathrm{NL}}} \right) \left(1 + \frac{\gamma_N^2}{\omega_{\mathrm{ro}}^2 + [\gamma_n + \gamma_{\mathrm{NL}}]\gamma_N} \right), \qquad (23)$$

which is the central result of this section. The noise threshold behavior will now generally depend on both γ_N and γ_{NL}, so that the description is somewhat more complicated than that of Sec. III A, and the ratio

$$\frac{\gamma_{\mathrm{NL}}}{\gamma_n} = \frac{\gamma_a \beta n_0 (n_0 + 1)}{\gamma_b} \approx \frac{\beta n_0^2 \gamma_a}{\gamma_b} \qquad (24)$$

is now a third key quantity, in addition to Eqs. (8) and (9). As parameters, we deal now with β, Λ, and $\Lambda' \equiv \gamma_b / \gamma_a$. Several simplifications are possible, however.

Firstly, it should be noted that around the steady-state threshold ($M \approx 1, n_0 \approx \beta^{-1/2}$), Eq. (24) yields $\gamma_{\mathrm{NL}} \ll \gamma_n$, since $\gamma_a \ll \gamma_b$. Thus, around the steady-state threshold Eq. (6) is an excellent approximation to Eq. (23). This leads to the conclusion that the ''macroscopic'' and ''mesoscopic'' regimes are hardly affected by the damping term γ_{NL} associated with the lower-level dynamics; two parameters are adequate.

Secondly, for the ''microscopic regime'' the situation simplifies when γ_N is negligible compared to $\gamma_n + \gamma_{\mathrm{NL}}$ for all relevant pump powers, as is the case in our experiments. In that case γ_{NL} replaces γ_N, and we have $Q_2 \approx \gamma_n / (\gamma_n + \gamma_{\mathrm{NL}})$. Since the ratio of Eq. (24) is directly analogous to the approximate expression for γ_N / γ_n in the microscopic regime, Eq. (18), the behavior of Q_2 and F is directly analogous to the microscopic regime described in Sec. III A [e.g., Eq. (19)] once $\Lambda = \Gamma_c / \gamma_\parallel$ is replaced by $\Lambda' = \gamma_b / \gamma_a$. Again, two parameters are adequate.

IV. COMPARISON WITH EXPERIMENTAL RESULTS

In this section, we compare the experimental results, obtained with the setup of Sec. II, to the theory of Sec. III. We start by describing the experimental data. Typical experimental time traces of the output power P_{out} and RF spectra of the intensity noise are shown in Fig. 5. Note how a reduction of the pump power P_{pump} changes the laser output from reasonably stable with well-behaved relaxation oscillations, Figs. 5(a), 5(b), via strongly anharmonic relaxation oscillations, Figs. 5(c), 5(d), to highly irregular, Figs. 5(e), 5(f).

The output characteristics of the laser are extracted from these data, and are summarized in Fig. 6, as a function of normalized pump parameter $M = P_{\mathrm{pump}} / P_{\mathrm{thr}}$. Figure 6(a) shows the average output power, converted into units of intracavity photon number in the lasing mode n. The data exhibit a sharp threshold (as the inset shows in more detail), at $M = 1 (P_{\mathrm{thr}} = 17.3$ mW). This sharpness is as expected, since β is relatively small.

Figures 6(b) and 6(c) show the photon number fluctuations, represented both as the Fano factor F and the reduced factorial moment Q_2. Clearly, the observed behavior of our laser deviates significantly from that expected on the basis of conventional laser theory [see Figs. 4(a) and 4(b)]. The fluctuations are much stronger, and decrease only very slowly as the pump power is increased, i.e., the intensity fluctuations

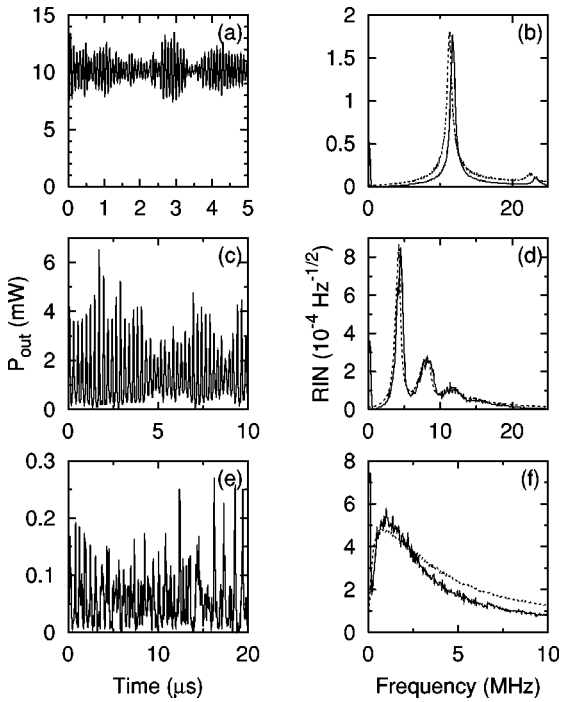

FIG. 5. Typical experimental time traces (left) and RF spectra (right, solid curves) of the output of the microchip laser, for different pump parameters $M = P_{\mathrm{pump}} / P_{\mathrm{thr}}$. (a), (b): $M = 6.6$; (c), (d): $M = 1.9$; (e), (f): $M = 1.03$. The RF spectra are normalized to the average output power, to yield the relative intensity noise (RIN). The dashed curves in the spectra are the result of numerical integration of Eqs. (20).

have become thresholdless, as in Figs. 4(g) and 4(h). The intensity fluctuations are highly super-Poissonian above threshold, the Fano factor reaching a value of almost 10^5 at $M = 2$, much larger than the peak value $\beta^{-1/2}$ (≈ 400 in our case) at $M = 1$, expected for a class-A laser.

The fluctuations are centered around the relaxation-oscillation frequency ω_{ro}, as is characteristic for class-B lasers. This frequency was extracted as the principal harmonic component of the RF spectra, and is plotted in Fig. 6(d). Another important parameter is the width (FWHM) of the principal relaxation-oscillation peak in the RF spectra $\Delta\omega_{\mathrm{ro}}$. It is usually a good measure for the damping rate of the relaxation oscillations, and is plotted in Fig. 6(e).

To quantitatively compare our experimental data to the linearized model we have used the following procedure: the value of β was determined by fitting $n_0 \approx (M-1)/\beta$ to the data of Fig. 6(a) in the region $M \lesssim 3$, and the value of Γ_c was determined by fitting $\omega_{\mathrm{ro}} \approx [\gamma_\parallel \Gamma_c (M-1)]^{1/2}$ to the data of Fig. 6(d), using the separately measured value of $\gamma_\parallel$. The resulting fits are shown as solid curves in Figs. 6(a), 6(d), and yield the values $\beta = 7 \times 10^{-6}$ and $\Gamma_c = 7 \times 10^{10}$ s^{-1} respectively, in satisfactory agreement with the estimated values of Sec. II. Combining these values with the value for $\gamma_b = 1.6 \times 10^9$ s^{-1} from Ref. [9], we obtain the solid curves for the Fano factor F, for the reduced factorial moment Q_2 and for the relaxation-oscillation damping γ_{ro} shown in Figs. 6(b), 6(c), and 6(e). For our laser, the atomic damping is dominated by the lower-level dynamics (since $\Gamma_c \gg \gamma_b$), and

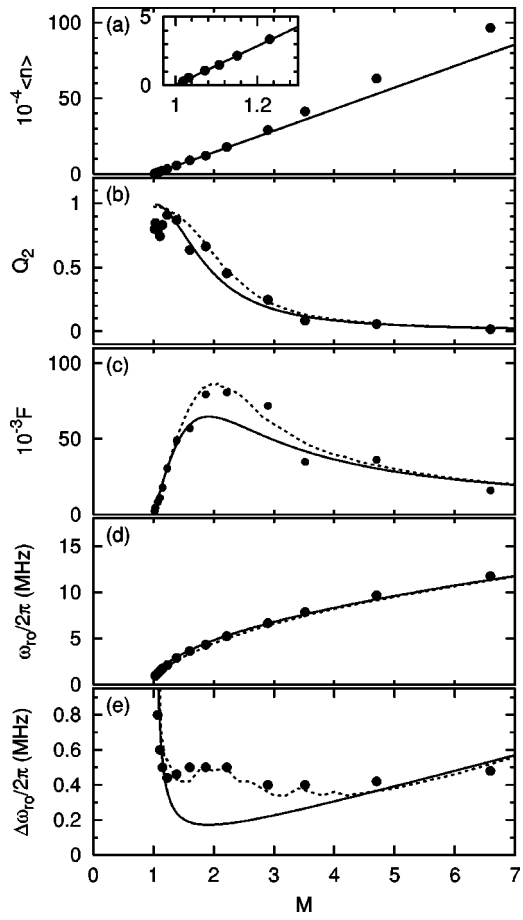

FIG. 6. Threshold characteristics of the slow-inversion laser, as a function of pump parameter $M=P_{\text{pump}}/P_{\text{thr}}$. The experimental data are given by the solid circles (●), the solid curves are based on the linearized rate equations; the dashed curves result from numerical integration of Eqs. (20). (a) Average intracavity photon number in the lasing mode, the inset shows the threshold region in more detail; note that the numerical data are not visible because they overlap with the linearized theory. (b) Photon-number fluctuations, as parameterized by the reduced factorial moment Q_2 and (c) by the Fano factor F. (d) Principal relaxation-oscillation frequency and (e) width (FWHM) of the principal relaxation-oscillation peak.

the point $\gamma_n \approx \gamma_{\text{NL}}$ is reached around $M \approx 1+(\beta\gamma_b/\gamma_\parallel)^{1/2} \approx 2$. Clearly, our linearized model describes quantitatively most features of the experimental data. In Fig. 6, the only significant discrepancy is in the region $M \approx 2$ in Fig. 6(e), where the experimentally observed width $\Delta\omega_{\text{ro}}$ of the relaxation-oscillation peak deviates from the value of $2\gamma_{\text{ro}}$ for the linearized theory.

In fact, the agreement between linearized model and experiment is surprising, since the linearization must break down in the regime of interest, where the fluctuations in the photon number are comparable to its mean value. The appearance in the RF spectra of harmonics of the relaxation oscillation frequency, for instance, can not be described by the linearized equations. Analytical attempts to solve the nonlinearized Eqs. (1) [or Eq. (20)] have met with only modest success [19–21]. We have therefore resorted to numerical integration of Eqs. (20), after adiabatic elimination of N_b. The resulting time traces were transformed into RF spectra by applying a fast Fourier-transform (FFT) algorithm, and averaging the result for several time traces. Examples of the numerically obtained RF spectra are shown in Fig. 5, and the extracted threshold behavior is summarized in Fig. 6 (dashed curves). These numerical data reproduce the experimental data to within the experimental error bars. In particular, we find agreement in the strength and shape of the harmonics of the relaxation oscillations, and in the behavior of $\Delta\omega_{\text{ro}}$ around $M=2$.

The failure of the linearized theory in describing the width of the relaxation-oscillation peak $\Delta\omega_{\text{ro}}$ is due to the fact that it does not take into account anharmonicity: the relaxation oscillation period increases for large amplitudes [19]. Because of this, the fluctuating amplitude of the relaxation oscillations (see Fig. 5) results in a fluctuating relaxation-oscillation frequency (decreasing for larger amplitudes), leading to an increased width (beyond that due to damping) of the principal relaxation-oscillation peak in the RF spectra. This explains the behavior of the experimental and numerical $\Delta\omega_{\text{ro}}$ around $M=2$ in Fig. 6(e). It also leads to the slight downward shift in the principal relaxation-oscillation frequency that is visible in the numerical data of Fig. 6(d), when compared to the curve of the linearized theory.

V. DISCUSSION AND CONCLUSION

Figure 3 illustrates the key point of the results presented here: there is a large, and experimentally accessible range of laser parameters where the conventional, ''macroscopic'' noise threshold no longer applies. In the ''microscopic'' regime, the intensity noise becomes effectively thresholdless. We emphasize that the distinction between these regimes is not identical to the distinction between class-A and class-B lasers. The latter distinction is purely based on Λ $(=\Gamma_c/\gamma_\parallel)$; $\Lambda<1$ for class-A lasers and $\Lambda>1$ for class-B lasers. Whereas class A lasers always operate in the conventional, ''macroscopic'' regime, class-B lasers may operate in any of the three regimes, depending on the value of β. The current trend towards smaller laser devices leads to lasers with increased β and Λ (Λ increases because typically $\gamma_\parallel$ is a material property of the gain medium while Γ_c increases with decreasing cavity length). Thus, this trend will naturally lead to lasers that have ''mesoscopic'' or even ''microscopic'' intensity fluctuations.

Our results seem particularly relevant for the ongoing efforts towards $\beta=1$, where the *average* intensity becomes thresholdless. Most of these attempts employ semiconductor class-B lasers [6], thus we expect the intensity fluctuations of such lasers to first become thresholdless in the manner described here, at values of β considerably below 1. Indeed, Hofmann and Hess [13,14] argue that conventional semiconductor lasers already operate in the ''mesoscopic,'' or even the ''microscopic'' regime.

The analysis here has concentrated on the regime $\beta \ll 1$, where a semiclassical treatment suffices. Therefore, strictly speaking the extension towards $\beta=1$ of the different regimes in Fig. 3 is an extrapolation. The validity of this ex-

trapolation will have to be verified by a more rigorous (quantum) theory. In this regard it is interesting that from a numerical treatment of a quantum birth-death model for a $\beta=1$ laser with $\Lambda\gg1$, Rice and Carmichael [5] find scaling laws that closely resemble our analytical results. This strongly suggests that the extrapolation of our results towards $\beta=1$ is meaningful. For instance, they find $F_{\max}\approx0.6\Lambda^{1/2}$ at $\langle n\rangle\approx1.6\Lambda^{1/2}$ [see the discussion of Fig. 8(b) in Ref. [5], where $\lambda\equiv\Lambda$], directly analogous to our results in the microscopic regime [see Sec. III A, inserting $\beta=1$ in Eq. (19) yields $F_{\max}\approx0.5\Lambda^{1/2}$ at $n_0\approx M\approx\Lambda^{1/2}$].

Another demonstration of the surprising robustness of the linearized semiclassical treatment has already been pointed out in Sec. IV: the linearized approach should break down as soon as the fluctuations in intensity become comparable to the average. This is by definition the case when $Q_2\approx1$, i.e., precisely in the regime of interest. Our experimental and numerical results show that the predictions of the linearized treatment can nevertheless be accurate, and certainly serve as a convenient guideline and a powerful analytical tool.

According to Eq. (13), the ''microscopic'' regime where the intensity fluctuations become effectively thresholdless is reached for $\beta\Lambda\gtrsim1$. Interestingly, there is a direct connection with the common classification scheme in cavity QED, where one compares g, the atom-field coupling strength ($2g$ is the vacuum Rabi frequency), to the intrinsic decay rates of the system [22]. The above condition implies that $2g\gg\gamma_\parallel$, as can be easily verified using $\beta=2g^2/\gamma_\parallel\gamma_\perp$ [15], and noting that we have limited ourselves to the good-cavity regime, $\gamma_\perp\gg\Gamma_c$. Indeed, from this equation for β we find for our laser $g\approx10^5\ \mathrm{s}^{-1}\gg\gamma_\parallel$.

In conclusion, we have shown that the intensity fluctuations (second-order coherence) of a sufficiently small slow-inversion laser become thresholdless in the ''microscopic'' regime defined by Eq. (13), where the average intensity can still show a sharp threshold. It would be highly interesting to study also the first-order coherence, and we are currently working along that line.

ACKNOWLEDGMENTS

We thank Jos Dingjan for measuring the fluorescence linewidth of the laser crystal. The research of N. J. van Druten has been made possible by the ''Koninklijke Nederlandse Akademie van Wetenschappen.'' We acknowledge support from the Foundation FOM, and from the European Union under the TMR Contract No. ERB4061PL95-1021 (Microlasers and Cavity QED).

APPENDIX: INFLUENCE OF INVERSION NOISE

Here, we discuss in some more detail the influence of inversion noise. Including a noise source $f_N(t)$ in Eq. (1b) leads to the appearance of f_N in Eq. (3b). Fourier transforming and inverting the resulting matrix equation yields

$$\delta n(\omega)=\frac{(\gamma_N-i\omega)f_n(\omega)-\gamma_\parallel\beta(n_0+1)f_N(\omega)}{\omega_{\mathrm{ro}}^2+\gamma_n\gamma_N-\omega^2-2i\omega\gamma_{\mathrm{ro}}}. \quad \text{(A1)}$$

The key point is now that the denominator in Eq. (A1) causes δn to be resonantly enhanced around the relaxation oscillation frequency $\omega\approx\omega_{\mathrm{ro}}\gg\gamma_\parallel$. At that frequency the photon noise source f_n shows up in δn with a much larger prefactor ($\approx\omega_{\mathrm{ro}}$) than the inversion noise f_N (note that βn_0 is of order unity or smaller). For instance, for a Poissonian pump source, one has $\langle f_N(t)f_N(t')\rangle=2\gamma_\parallel N\delta(t-t')$ [15], and it can be readily shown that the contribution of f_n to the spectral density $\langle\delta n^2(\omega)\rangle$, is $\Lambda(\gg1)$ times larger than the contribution of f_N.

Equation (A1) also shows that for frequency-resolved measurements at low frequencies $\omega\approx\gamma_\parallel$ the pump noise could be important. In fact, Hofmann and Hess [14] argue that at these frequencies a slow-inversion laser will display amplitude squeezing below the shot-noise limit for a sufficiently regular pump source.

We now address the *technical* pump noise. Fluctuations in the pump-beam intensity enter via the pump rate S, and thus contribute to the inversion noise source f_N. Denoting the bandwidth of the pump-intensity noise by γ_{pump}, and its relative root-mean-square value by $R\leqslant1$, the contribution to the spectral density of f_N is $R^2S^2/\gamma_{\mathrm{pump}}$ (for frequencies $\omega<\gamma_{\mathrm{pump}}$). The impact of the pump noise at the relaxation oscillation frequency can now easily be estimated by assuming (as a worst-case scenario) that the pump noise bandwidth extends up to or beyond the relaxation oscillation frequency ω_{ro}. In this case, the technical pump noise contribution to $\langle\delta n^2(\omega_{\mathrm{ro}})\rangle$ compared to the contribution of the ωf_n term is $R^2M^2\gamma_\parallel/2\beta\gamma_{\mathrm{pump}}$. This ratio is much smaller than 1 for our experiment (as mentioned in Sec. II we have $R\approx10^{-3}$), justifying our assumption that the technical pump noise may be neglected. For completeness we note that the technical pump noise mainly occurs at low frequencies ($\ll\omega_{\mathrm{ro}}$), so that the above in fact greatly overestimates the impact of the technical pump noise.

At low frequencies ($\omega\lesssim\gamma_\parallel$), the pump noise contribution should be compared to γ_Nf_n. The relative contribution of the technical pump noise to the spectral density of δn is now $\approx R^2\Gamma_cn_0/2\gamma_{\mathrm{pump}}$. As a result, at these frequencies the technical noise pump noise dominates in our experiment, and the predicted possibility of squeezing [14] will not be visible.

[1] M. Sargent III, M.O. Scully, and W.E. Lamb, Jr., *Laser Physics* (Addison-Wesley, Reading, 1974).
[2] R. Loudon, *The Quantum Theory of Light*, 2nd ed. (Oxford University Press, Oxford, UK, 1983).
[3] D.F. Walls and G.J. Milburn, *Quantum Optics* (Springer, Berlin, Germany, 1994).
[4] F.T. Arecchi, in *Instabilities and Chaos in Quantum Optics*, Vol. 34 of *Springer Series in Synergetics*, edited by F.T. Arecchi and R. G. Harrison (Springer, Berlin, 1987), pp. 9–48.
[5] P.R. Rice and H.J. Carmichael, Phys. Rev. A **50**, 4318 (1994).
[6] Y. Yamamoto and R.E. Slusher, Phys. Today **45**(6), 66 (1993).
[7] J.J. Zayhowski and A. Mooradian, Opt. Lett. **14**, 24 (1990).
[8] *Crystal Guide*, Casix Inc., Fuzhou, China, 1999.

[9] C. Becher and K.-J. Boller, J. Opt. Soc. Am. B **16**, 286 (1999).
[10] M.P. van Exter, G. Nienhuis, and J.P. Woerdman, Phys. Rev. A **54**, 3553 (1996).
[11] D.E. McCumber, Phys. Rev. **141**, 306 (1966).
[12] M. Lax, IEEE J. Quantum Electron. **3**, 37 (1967).
[13] H.F. Hofmann and O. Hess, Phys. Rev. A (to be published).
[14] H.F. Hofmann and O. Hess, J. Opt. Soc. Am. B (to be published) (e-print quant-ph/0002007).
[15] R.B. Levien, M.J. Collett, and D.F. Walls, Phys. Rev. A **47**, 5030 (1993).
[16] J. Arnaud, J. Opt. Soc. Am. B **14**, 2193 (1997).
[17] K. Petermann, *Laser Diode Modulation and Noise* (Kluwer Academic, Dordrecht, 1988).
[18] M. Willatzen, T. Takahashi, and Y. Arakawa, IEEE Photonics Technol. Lett. **4**, 682 (1992).
[19] G.L. Oppo and A. Politi, Z. Phys. B **59**, 111 (1985).
[20] P. Paoli, A. Politi, and F.T. Arecchi, Z. Phys. B **71**, 403 (1988).
[21] T. Ogawa, Phys. Rev. A **42**, 4210 (1990).
[22] *Cavity Quantum Electrodynamics*, Supplement 2 of *Advances in Atomic, Molecular, and Optical Physics*, edited by P.R. Berman (Academic Press, San Diego, 1994).